Theory for Concentration and Solvency Effects in Size-Exclusion Chromatography of Polymers

G. J. Fleer*

Laboratory for Physical Chemistry and Colloid Science, Wageningen University, 6703 HB Wageningen, Netherlands

A. M. Skvortsov

Chemical-Pharmaceutical Academy, Prof. Popova 14, 197022 St. Petersburg, Russia

Received November 29, 2004; Revised Manuscript Received January 12, 2005

ABSTRACT: A simple analytical equation for the distribution coefficient K in size-exclusion chromatography (SEC) as a function of molar mass, concentration, and solvent quality is presented. The theory is based upon a modified Casassa equation, using a recently proposed mean-field relation for the depletion thickness δ, which for better than Θ conditions reads $1/\delta^2 = 1/\delta_0^2 + 1/\xi^2$. Here δ_0 is the well-known (chain-length-dependent) depletion thickness at infinite dilution, and ξ is the (concentration- and solvency-dependent) correlation length in the solution. Numerical lattice calculations for mean-field chains in slitlike pores of width D as a function of concentration are in quantitative agreement with our analytical equation, both for good solvents and in a Θ solvent. Comparison of our mean-field theory with Monte Carlo data for the concentration dependence of K for self-avoiding chains shows qualitatively the same trends; moreover, our model can also be adjusted to obtain nearly quantitative agreement. The modified Casassa equation works excellently in the wide-pore regime (where $K = 1 - 2\delta/D$) and gives an upper bound for the narrow-pore regime. In fact, the simple form $K = 1 - 2\delta/D$ for $2\delta/D < 1$ and $K = 0$ for $2\delta/D > 1$ gives a first estimate of concentration effects even in the narrow-pore regime. A more detailed analysis of interacting depletion layers in narrow pores shows that a different length scale δ_i (the "interaction distance") enters, which in semidilute solutions is somewhat higher than δ, leading to a smaller K than that obtained with the wide-pore length scale δ. Predictions for the effects of chain length, solvency, and chain stiffness on the basis of our analytical equation are in accordance with Monte Carlo simulations.

1. Introduction

Size-exclusion chromatography (SEC) is a standard method for the separation and analysis of polymers.[1] It has been widely used to characterize the molar mass distribution and to prepare relatively homodisperse fractions from a polydisperse sample.[2−4] When the segments are repelled by the pore walls, the separation mechanism in dilute solutions is based upon the chain entropy: long chains lose more entropy than short ones upon entering the pores, and they are therefore more strongly excluded from the porous stagnant phase.

The basic theory describing this exclusion on the basis of chain length was constructed by Casassa,[5,6] who used the model of an isolated random-flight chain (with radius of gyration R) in a slitlike (or cylindrical) pore of width D. In this model, the partition coefficient K (which is the ratio of the average concentration $\bar{\varphi}$ inside the pore and the outside bulk solution concentration φ_b in the mobile phase) is determined only by the ratio R/D. Casassa's theory was verified many times by experiment[7,8] and by computer simulations:[9−11] in dilute solutions (below the overlap concentration) the partitioning is governed by this ratio R/D, not only under Θ conditions (where $R \propto N^{1/2}$ as for random-flight chains) but also for good solvent conditions (where $R \propto N^{3/5}$ due to intramolecular excluded-volume effects).

For separating a finite amount of polydisperse polymer under dilute conditions, a large amount of solvent is required.[1] Moreover, recovery of the (very) dilute fractions to obtain fractionated samples is inefficient. Therefore, in preparative SEC long columns and high concentrations (overlapping coils) are used.[12] These preparative methods are known as "enhanced partitioning fractionation" or "high-osmotic-pressure chromatography".[13−16] However, under these conditions the concentration is so high that the original Casassa theory no longer works. In addition, solvency effects show up; there are indications that high-osmotic-pressure chromatography gives better separation in a Θ solvent.[17] It is therefore important to have a theory for concentration and solvency effects in SEC.

In the literature there is extensive evidence of such concentration effects. Satterfield et al.[18,19] observed a strong increase with mobile-phase concentration of the partition coefficient K for monodisperse samples of polystyrene in two solvents (chloroform and dichloroethane) with porous glass as the stationary phase. A similar effect was observed by Brannon and Anderson[20] for dextran and controlled-pore glass. Teraoka et al.[15,21] found that K increases with concentration for monodisperse polystyrene on porous silica.

Several theoretical approaches have been proposed to account for this concentration effect on the partition coefficient K. Rudin[22] and Bleha et al.[23] tried to explain the increase of K on the basis of the reduction in the coil dimension with increasing concentration, which is known to occur in good solvents but not in a Θ solvent.[24] However, their theoretical estimates for the increase of K in a good solvent are much smaller than the experimental observations, and their theory fails to explain the increased partition coefficient in a Θ solvent.

In a second type of theory the polymer coils are modeled as a hard spheres.[25−27] The second virial coefficient of such a hard-sphere dispersion, calculated from the Ornstein−Zernike equation for dense liquids,

* Corresponding author. E-mail Gerard.Fleer@wur.nl.

10.1021/ma047542b CCC: $30.25
Published on Web 02/18/2005

was interpreted to reflect the partition coefficient. In these approaches, the distribution coefficient K has to be evaluated numerically for different sphere and pore sizes. A higher dispersion concentration drives the hard spheres into the pores. However, the predicted dependencies differ from the experimental observations. Hard-sphere theory predicts that narrow pores (with diameter smaller than the sphere diameter) cannot be entered at all (implying that K is zero for any concentration), whereas there is experimental evidence[15,18−21] that K increases with concentration also for narrow pores. Therefore, hard-sphere theory cannot explain the experimental facts. It certainly cannot cope with (experimentally verified) solvency effects.

Considerable progress as to the concentration effect on K was obtained in Monte Carlo (MC) simulations on a lattice.[10,11,28−35] The distribution coefficient, the density profiles in a slitlike pore, and different global and local characteristics (end-to-end distance, radius of gyration, coil anisotropy, fraction of gauche and trans bonds) as a function of concentration were calculated for both athermal and Θ solvents. Also, the effect of chain flexibility was studied.[36,37] The overall trend is that K is small at low concentrations and increases strongly in a relatively narrow concentration region (the so-called weak-to-strong penetration[11]), after which a more gradual increase is found. There is a strong effect of solvency: in a Θ solvent the transition is steeper and occurs at a higher concentration than in a good solvent.

Teraoka and Wang[38] developed a mean-field Gaussian chain theory to interpret the simulation results for a good solvent. They used an approximate expression for the osmotic pressure of chains with short-range repulsive interactions and were able to numerically evaluate K as a function of concentration. However, no attempt was made to quantitatively compare with the MC data.

Teraoka and Cifra[39] proposed a model for a Θ solvent. They applied cluster theory for the free energy in the bulk solution[40] to define an effective potential field for the chains. The effect of polymer concentration was included by a semiempirical formula. Again, the results had to be evaluated numerically; no closed analytical form for K was obtained. The distribution coefficient was found to first decrease with concentration and then sharply increase. This initial decrease must be related to some deficiency in the model.

So the present state of the art for describing concentration and solvency effects in SEC is far from satisfactory. The aim of the present paper is to present a simple analytical model for the distribution of polymer over slitlike pores and a bulk solution. On the mean-field level, an exact numerical self-consistent-field (SCF) lattice theory due to Scheutjens and Fleer[41] is available. We were able to find an analytical simplification of this model for the case of depletion, which describes the exact data very well. The starting point is a recently proposed equation[42] for the depletion thickness δ at a single surface as a function of chain length, concentration, and solvency. This equation describes the partition coefficient in wide slitlike pores, where the depletion layers do not overlap very precisely. The model can also be extended to narrow pores by modifying the original Casassa theory for ideal chains. Moreover, we will show that our mean-field model can be adjusted to also describe the simulation data for MC chains.

This paper is organized as follows. In section 2 we briefly review the relevant equations for the single-wall depletion thickness δ. In (very) dilute solutions its value δ_0 depends only on the chain length N, but at finite concentrations it decreases and becomes a function of concentration and solvency. In section 3 we summarize the original Casassa theory (in terms of the ratio δ_0/D), and we propose a modified Casassa equation by replacing $\delta_0(N)$ by $\delta(N,\varphi_b,\chi)$, where χ is the Flory−Huggins solvency parameter. In section 4 we test our model against exact SCF computations for mean-field (MF) chains. In section 5 we show that the MC simulations for self-avoiding chains by Cifra et al.[11] may be interpreted along the same lines. In section 6 we illustrate that both the MF results and the MC data may be described by "modified Casassa master plots" in terms of δ/D, where the functional dependence $\delta(\varphi_b,\chi)$ is extracted from wide-pore data. In section 7 we address some subtleties occurring in the narrow-pore regime for finite concentrations. Finally, in section 8 we present some predictions as to the effect of chain length, solvency, and chain stiffness.

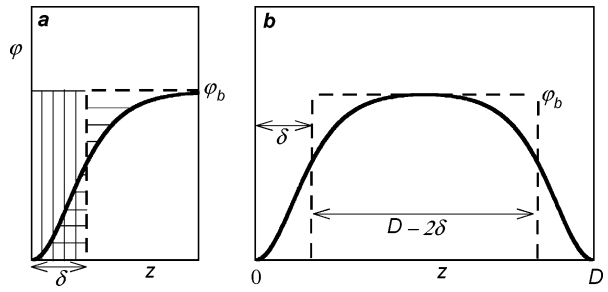

Figure 1. Concentration profile $\varphi(z)$ near a single wall (a) and in a wide slit of width D (b). The depletion thickness δ is indicated (vertical dashed lines). In (a) the horizontally shaded areas left and right of $z = \delta$ are equal, and the vertically shaded area is minus the negative adsorption Γ, which is given by $-\Gamma = \varphi_b\delta$. In (b) a fraction $(D - 2\delta)/D$ of the pore volume is available for the polymer.

2. Depletion Thickness

In Figure 1 we sketch the polymer concentration profile $\varphi(z)$ next to a single (repulsive) wall (Figure 1a) and in a slit of width D that is wide enough for $\varphi(D/2)$ in the middle of the slit to be equal to the bulk concentration φ_b (Figure 1b). For wide slits the profile over half of the slit is identical to that at a single surface. Figure 1 is drawn for the boundary condition $\varphi(0) = \varphi(D) = 0$, which is the usual assumption in continuum models.

The depletion thickness δ is the zeroth moment of the profile (dashed vertical line in Figure 1a), such that the two horizontally shaded areas in Figure 1a are equal. The negative adsorption Γ is minus the vertically shaded area $\delta\varphi_b$ in Figure 1a. Hence, the depletion thickness δ is directly coupled to Γ:

$$\delta = -\Gamma/\varphi_b \tag{2.1}$$

The depletion thickness may also be related to the partition coefficient in a wide pore. Generally, K is defined as $K = \bar{\varphi}/\varphi_b$, where $\bar{\varphi}$ is the average concentration in the pore. From Figure 1b it is obvious that in wide pores $\bar{\varphi}$ is smaller than φ_b by a factor $(D - 2\delta)/D$. Hence

$$K = 1 - \frac{2\delta}{D} \qquad \delta = \frac{D}{2}(1 - K) \tag{2.2}$$

In very dilute solutions of ideal chains consisting of N segments, which have a radius of gyration $R = \sqrt{N/6}$ (in units of the bond length l), the profile $\varphi_e(z)$ of the chain end points next to a repulsive wall is given by $\varphi_e/\varphi_b = \mathrm{erfc}(z/2R)$; the overall profile is a slightly more complicated function of $z/2R$.[43,44] From integration over these profiles (with boundary condition $\varphi(0) = 0$), the depletion thickness δ_0 in this dilute limit turns out to be somewhat larger than R:[6,43,44]

$$\delta_0 = \frac{2}{\sqrt{\pi}} R = \sqrt{\frac{2N}{3\pi}} \tag{2.3}$$

In this dilute limit $\delta = \delta_0$ is only a function of the radius of gyration (which depends on chain length).

For finite concentrations, the depletion thickness δ is smaller than δ_0 because the increasing osmotic pressure of the bulk solution pushes the chains closer toward the surface. Now the profile is rather accurately described by $\varphi(z)/\varphi_b = \tanh^2(z/\delta)$.[42,45] We note that $\varphi(z)/\varphi_b = \tanh^2(z/\delta_0)$ with δ_0 given by eq 2.3 is also a good approximation for the exact profile in terms of erfc-$(z/2R)$ in the dilute limit.[42,46]

Because the osmotic pressure depends on φ_b and on the solvency parameter χ, δ becomes also a function of φ_b and χ. Recently,[42,47] we derived the following mean-field expression for $\delta(N,\varphi_b,\chi)$:

$$\frac{1}{\delta^2} = \frac{1}{{\delta_0}^2} + \frac{1}{(p\xi)^2} \tag{2.4}$$

Here, the parameter p is unity in a good solvent ($\chi < 0.45$) and $p = \sqrt{3/2}\ \mathrm{atanh}(1/\sqrt{3}) \approx 0.81$ in a Θ solvent. The length ξ is a (generalized) correlation length in the solution and is (in units l) given by

$$\frac{1}{\xi^2} = -3\ln(1-\varphi_b) - 6\chi\varphi_b = 3v\varphi_b + \frac{3}{2}{\varphi_b}^2 + \ldots \approx \begin{cases} 3\varphi_b\ (\chi = 0) \\ \frac{3}{2}{\varphi_b}^2\ (\chi = 0.5) \end{cases} \tag{2.5}$$

where $v = 1 - 2\chi$ is the Edwards excluded-volume parameter, which is unity for an athermal solvent ($\chi = 0$) and zero for a Θ solvent ($\chi = 0.5$). In very dilute solutions ($\varphi_b \to 0$, $\xi^{-2} \to 0$) we have from eq 2.4 $\delta = \delta_0$ as in eq 2.3, for semidilute solutions $\delta = p\xi$, which scales as ${\varphi_b}^{-1/2}$ in a good solvent and as ${\varphi_b}^{-1}$ in a Θ solvent. Actually, this limiting form $\delta = p\xi$ is the high-N limit of δ even in rather dilute solutions; in this limit δ no longer depends on chain length.

Previously,[42] we tested eq 2.4 against full numerical lattice computations using the Scheutjens−Fleer model. Excellent agreement was found, provided the segment−wall repulsion in the lattice model is chosen such that the boundary condition $\varphi(0) = 0$, which is used in continuum models and is also the basis of eq 2.4, is satisfied. In a continuum model the segments occupy no volume and can approach the wall to distances smaller than l; then $\varphi(0) = 0$ corresponds to a strongly repelling surface. In a discrete model the shortest distance of approach is $z = {}^1/_2$ (in units l) for the center of the segments. When now infinite repulsion is assumed (i.e., the adsorption energy parameter χ_s is $-\infty$), the first solution layer is empty, which may be translated as $\varphi({}^1/_2) = 0$. To find $\varphi(0) = 0$ in a lattice model with finite segment size, the repulsion has to be less strong. In the appendix of ref 42 the boundary conditions in the continuum and lattice models were compared, and it was derived which value of χ_s has to be chosen in the lattice model to obtain $\varphi(0) = 0$. The result is

$$\chi_s = -(\chi + \Delta\chi)/6 \tag{2.6}$$

where $\Delta\chi$ is the difference between the polymer−wall Flory−Huggins parameter χ_{PW} and the polymer−solvent interaction χ. It was shown that in not too concentrated solutions (below about 10%) $\Delta\chi$ is a constant: $\Delta\chi = 6\ln({}^7/_6) \approx 1$. In the present paper we will also consider more concentrated systems where $\Delta\chi$ becomes a function of concentration and solvency. Then[42]

$$\frac{\Delta\chi}{6} = \ln\left(\frac{4}{6} + \frac{1}{6}\sqrt{\frac{\varphi_2}{\varphi_1}}\right) + \ln\frac{1-\varphi_1}{1-\varphi_b} + \frac{\chi}{3}(4\varphi_1 + \varphi_2 - 6\varphi_b) \tag{2.7}$$

where $\varphi_1 = \varphi_b \tanh^2(0.5/\delta)$ and $\varphi_2 = \varphi_b \tanh^2(1.5/\delta)$ are the concentrations in the first ($z = 0.5$) and second ($z = 1.5$) layers, respectively, for a concentration profile which extrapolates to $\varphi(0) = 0$. For relatively dilute solutions only the first term is relevant; with $\varphi_2/\varphi_1 = \tanh^2(1.5/\delta)/\tanh^2(0.5/\delta) \approx (1.5/0.5)^2 = 9$ eq 2.7 leads to the constant value $\Delta\chi = 6\ln({}^7/_6)$ mentioned above. For higher concentrations, $\Delta\chi$ increases with φ_b.

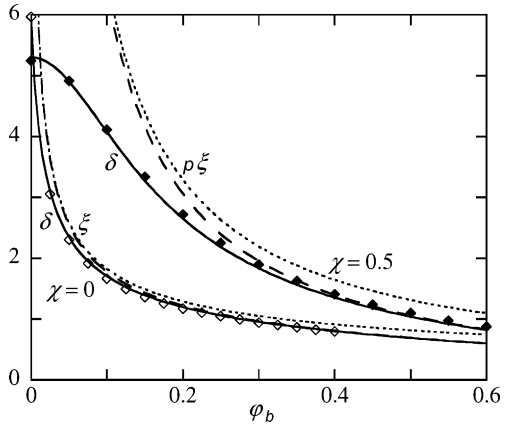

Figure 2. Depletion thickness δ (solid curves, symbols) and its high-N limit $p\xi$ (dashed, dotted) for $\chi = 0$ and $\delta_0 = 6$ (lower curves) and for $\chi = 0.5$ and $\delta_0 = 5.3$ (upper curves), as a function of the polymer concentration φ_b. The symbols are exact numerical SCF results for $N = (3\pi/2)\delta_0^2$ ($N = 170$ for $\chi = 0$ and $N = 132$ for $\chi = 0.5$) and χ_s as given by eqs 2.6 and 2.7. The solid curves were computed with eqs 2.4 and 2.5. The dashed curves give $p\xi$ (with $p = 1$ for $\chi = 0$ and $p = 0.81$ for $\chi = 0.5$) with for ξ the full logarithmic form of eq 2.5a. For the dotted curves the limiting forms of eq 2.5c were used.

Figure 2 gives an example of $\delta(\varphi_b)$ for two solvencies, $\chi = 0$ (athermal) and $\chi = 0.5$ (theta). In this example we chose $\delta_0 = 6$ for $\chi = 0$ and $\delta_0 = 5.3$ for $\chi = 0.5$. These numbers allow a comparison with Cifra's MC simulations,[11] to be discussed in Figures 6−9. The solid curves in Figure 2 show δ according to eq 2.4, with $p = 1$ for $\chi = 0$ and $p = 0.81$ for $\chi = 0.5$. The symbols are numerical SCF computations, with chain lengths $N = (3\pi/2)\delta_0^2$ (i.e., $N = 170$ for $\chi = 0$ and $N = 132$ for $\chi = 0.5$) and $\Delta\chi$ values as computed from eq 2.7. There is excellent agreement between the simple analytical form of eq 2.4 and the exact numerical data. It is clear that δ is smaller in a good solvent as compared to a Θ solvent due to the higher osmotic pressure. Only for very dilute solutions

($\varphi_b < 0.002$) is δ higher in the good solvent because of the higher δ_0.

For comparison, we plotted in Figure 2 also $p\xi$, which is the high-φ_b limit of δ, both with the full logarithmic form for ξ according to eq 2.5 (dashed curves) and with the expanded forms $\xi = (3\varphi_b)^{-1/2}$ for $\chi = 0$ and $\xi = \sqrt{2/3}\varphi_b^{-1}$ for $\chi = 0.5$ (dotted). For $\chi = 0$, $\delta = \xi$ with the logarithmic form for ξ applies above $\varphi_b \approx 0.15$ for this chain length; the expanded form gives a slight overestimation in concentrated solutions. For $\chi = 0.5$, $\delta = p\xi$ with the full form for ξ is only accurate above $\varphi_b \approx 0.5$, where the expanded form is significantly too high. We repeat that for large N the form $\delta = p\xi$ (dashed curves in Figure 2) applies also to (relatively) dilute solutions.

3. Analytical Form for the Partition Coefficient

3.1. Casassa Equation. We briefly review the classical Casassa theory[5,6] for the partition coefficient $K_0 = \bar{\varphi}/\varphi_b$ in a slitlike pore of width D with average inside concentration $\bar{\varphi}$ in equilibrium with an outside bulk solution with concentration φ_b in the dilute limit. We express the result in terms of the single-wall depletion thickness δ_0, which in the dilute limit is given by $\delta_0 = (2/\sqrt{\pi})R$ (eq 2.3). As for the depletion thickness, we use also for the partition coefficient the subscript 0 to indicate the dilute limit.

In Casassa's theory the partition coefficient K_0 is only a function of the ratio δ_0/D:

$$K_0 = \frac{8}{\pi^2}\sum_{n=1,3,\ldots}\frac{1}{n^2}\mathrm{e}^{-\pi^3(n\delta_0/2D)^2} = \begin{cases} 1 - \dfrac{2\delta_0}{D} & \dfrac{2\delta_0}{D} < 0.5 \\ \dfrac{8}{\pi^2}\mathrm{e}^{-\pi^3(\delta_0/2D)^2} & \dfrac{2\delta_0}{D} > 0.5 \end{cases} \quad (3.1)$$

As in eqs 2.3 and 2.4, the boundary condition for eq 3.1 is zero concentration at the pore walls.

The infinite sum of eq 3.1a has two limiting forms, which are given in eq 3.1b. In the narrow-pore regime ($K_0 < 0.5$) the first term ($n = 1$) of the sum suffices; in the wide-pore regime ($K_0 > 0.5$) eq 2.2 (with $\delta = \delta_0$) is recovered. For $2\delta_0/D = 0.5$ both limits apply: the wide-pore limit gives $K_0 = 0.500$, and the narrow-pore limit leads to $K_0 = (8/\pi^2)\exp(-\pi^3/64) = 0.499$, so the two limiting forms cross over very smoothly and the second form of eq 3.1 is nearly exact.

Figure 3 (curve labeled "low φ_b") gives a plot of K_0 as a function of $2\delta_0/D$ according to eq 3.1. The linear dependence for $2\delta_0/D < 0.5$ (which extrapolates to $K_0 = 0$ for $2\delta_0/D = 1$; see the dotted line in Figure 3) describes the wide-pore regime where the two depletion layers do not interact (compare Figure 1b). The Gaussian tail for $2\delta_0/D > 0.5$ corresponds to the narrow-pore limit.

Equation 3.1 is appropriate when φ_b is so low that the polymer coils in solution do not overlap. Then the depletion thickness $\delta = \delta_0$ does not depend on the polymer concentration, and the partitioning process can be described as originating from the interaction of single Gaussian coils with the (repulsive) pore walls.

3.2. Modified Casassa Equation. It is a well-known experimental fact[18−20] that for higher concentrations (overlapping coils) the partition coefficient K is higher than below overlap. An example is given by the curves

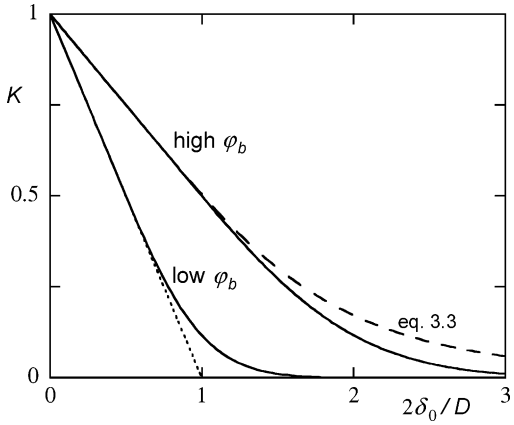

Figure 3. Partition coefficient K as a function of the ratio $2\delta_0/D$. The solid curve labeled "low φ_b" is K_0 according to the Casassa equation (eq 3.1); the dotted line is the extrapolation of its wide-pore limit $K_0 = 1 - 2\delta_0/D$. The solid curve labeled "high φ_b" is K according to the modified Casassa equation (eq 3.2), with in this case δ arbitrarily chosen as $\delta = \delta_0/2$. The dashed curve is the product function approximation of eq 3.3, again with $\delta = \delta_0/2$.

labeled "high φ_b" in Figure 3. The underlying reason for $K > K_0$ is that in relatively concentrated solutions the depletion thickness δ is smaller than the low-φ_b-limit δ_0, as discussed in section 2. Consequently, the polymer is able to penetrate more easily into the pores and K is higher; also here the increasing osmotic pressure is responsible.

In section 2 we discussed how (in mean-field) the depletion thickness δ depends on concentration and solvency. Knowing $\delta(N,\varphi_b,\chi)$, we propose a "modified Casassa equation" as a reference for K for finite concentrations. The modification is a simple replacement in eq 3.1 of the depletion thickness δ_0 for the dilute limit by the smaller depletion thickness δ above coil overlap:

$$K = \begin{cases} 1 - \dfrac{2\delta}{D} & 2\delta/D < 0.5 \\ \dfrac{8}{\pi^2}\mathrm{e}^{-\pi^3(\delta/2D)^2} & 2\delta/D > 0.5 \end{cases} \quad (3.2)$$

The solid curve labeled "high φ_b" in Figure 3 is drawn according to eq 3.2, with in this example (arbitrarily) $\delta = \delta_0/2$. This condition can be met by fixing the concentration (and thus δ) and varying the slit width D. When K would be plotted against $2\delta/D$, the curve would be identical to the "pure" Casassa result. When plotted against $2\delta_0/D$, as in Figure 3, there is a rescaling along the horizontal axis (in this example by a factor of 2), and at given δ_0 (or radius of gyration, or molar mass) the partitioning is weaker: K is higher (closer to unity).

This procedure of fixing φ_b and δ and changing the slit width is not readily accomplished in experimental situations, where it is easier to vary the concentration at fixed D. In that case the ratio δ/δ_0 is not constant because δ depends on concentration (see Figure 2). The conclusion that K is higher in more concentrated solutions remains valid also in this case, however.

Since in concentrated solutions δ is rather small, the ratio $2\delta/D$ may be below 0.5 even for relatively narrow pores (small D). Then the wide-pore regime ($K = 1 - 2\delta/D$) applies even for narrow pores. We therefore have to distinguish between the "narrow-pore regime" ($2\delta/D > 0.5$) and "narrow pores" (small D). We will consis-

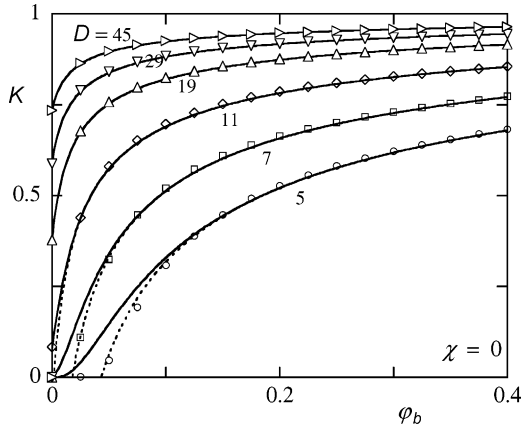

Figure 4. Numerical SCF data (open symbols) for the partition coefficient $K(\varphi_b)$ for $N = 170$ ($\delta_0 = 6$) in an athermal solvent ($\chi = 0$), for six slit widths D (indicated). The solid curves were calculated from the modified Casassa equation (eq 3.2), and the dotted curves for $D = 5$, 7, and 11 are the extrapolation of the wide-pore equation $K = 1 - 2\delta/D$. The quantity δ was obtained from eq 2.4 with $p = 1$.

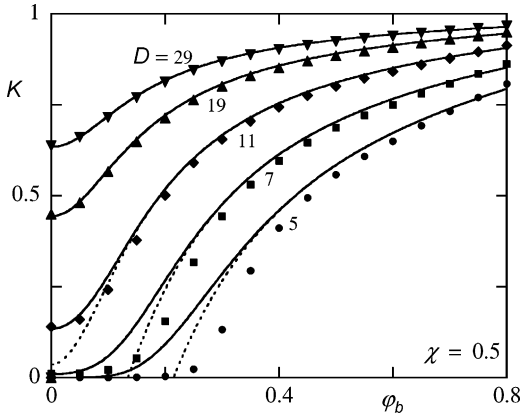

Figure 5. Numerical SCF data (filled symbols) for the partition coefficient $K(\varphi_b)$ for $N = 132$ ($\delta_0 = 5.3$) in a Θ solvent ($\chi = 0.5$), for five slit widths D (indicated). The solid curves were calculated from the modified Casassa equation (eq 3.2), and the dotted curves for $D = 5$, 7, and 11 are the extrapolation of the wide-pore equation $K = 1 - 2\delta/D$. The quantity δ was obtained from eq 2.4 with $p = 0.81$.

tently denote situations with $K < 0.5$ as the narrow-pore regime and those with $K > 0.5$ as the wide-pore regime, regardless of whether we have narrow or wide pores.

3.3. Product Function. In the literature a concentration profile in the slit has been proposed which allows to find an alternative expression for K. Tuinier and Lekkerkerker[48] introduced a "product function" approximation $\varphi(z)/\varphi_b = \tanh^2(z/\xi)\tanh^2[(D - z)/\xi]$ for semidilute solutions. The same form was later derived by Alexander-Katz et al.[49] from a mean-field ground-state approach. This profile may be integrated to find $\bar{\varphi}/\varphi_b = K$. When we replace ξ by δ, the result is

$$K = 1 - \frac{2\coth h}{h}\left(1 - \frac{2\ln\cosh h}{\sinh^2 h}\right) \qquad h = \frac{D}{\delta} \tag{3.3}$$

The dashed curve in Figure 3 gives a plot of K according to eq 3.3, again with $\delta = \delta_0/2$. The wide-pore behavior is the same as that of eq 3.2, but in narrow pores K is higher. We will see in the next section that the (modified) Casassa equation describes the exact SCF data in dilute systems very precisely and that deviations in more concentrated solutions always lead to a lower K and never to a higher value (see Figure 10 for MF chains and Figure 11 for MC chains). This implies that the product function overestimates the profile (and K) in narrow slits. Therefore, we will not use eq 3.3 and stick to our modified Casassa equation (eq 3.2).

4. Partition Coefficient for MF Chains

Figure 4 (open symbols) gives numerical SCF lattice results for the partition coefficient K as a function of concentration for a good solvent ($\chi = 0$) and a chain length $N = 170$ (corresponding to $\delta_0 = 6$), for six slit widths D; from top to bottom $D = 45$, 29, 19, 11, 7, and 5. These values were selected to be as close as possible to the Cifra data, to be discussed in the next section. The value of $\Delta\chi$ was chosen in accordance with eq 2.7 in order to ensure $\varphi(0) = \varphi(D) = 0$.

From Figure 4 it is clear that K increases with increasing concentration and increasing slit width. All data with $K > 0.5$ are in the wide-pore regime and should follow $K = 1 - 2\delta/D$ according to eq 2.2. For $D = 45$ and 29, even dilute solutions are in this regime: K starts at a value $K_0 = 1 - 2\delta_0/D = 1 - 12/D$ for $\varphi_b = 0$, and with increasing concentration K increases since δ becomes smaller than δ_0. For narrower pores the wide-pore regime, where at fixed φ_b (fixed δ) $1 - K$ is proportional to $1/D$, applies only to higher concentrations (smaller δ). For $D = 7$ and 5, K is close to zero at very low concentrations (below $\varphi_b \approx 0.02$ for $D = 7$ and $\varphi_b \approx 0.05$ for $D = 5$ in this example), but for higher φ_b the increasing osmotic pressure of the outside solution forces the polymer into the slit and K increases quickly with φ_b.

The solid curves in Figure 4 are drawn according to the modified Casassa equation (eq 3.2), with δ calculated from our simple analytical expression (eq 2.4). For the wide-pore regime ($K > 0.5$), where eq 3.2 reduces to $K = 1 - 2\delta/D$, the agreement is nearly perfect. This is because the analytical and numerical δ's agree very well (see Figure 2). For narrow pores, where $K = (8/\pi^2)\exp[-\pi^3(\delta/2D)^2]$ according to eq 3.2, the trends are still described rather well, even though for small K in narrow slits this equation overestimates the numerical partition coefficient. In section 7 we will discuss the origin of this overestimation.

When we extrapolate the wide-pore equation $K = 1 - 2\delta/D$ all the way to $K = 0$, the resulting curves (dashed in Figure 4) are very close to the numerical data. We shall return to this point in section 7. For the moment we conclude that using only the single-wall depletion thickness δ (eq 2.4) gives a nearly complete description of the numerical SCF data for K, not only in wide pores (which is to be expected) but also in narrow ones (which is somewhat surprising).

Figure 5 gives similar SCF data (filled symbols) for a Θ solvent, in this case for $N = 132$ ($\delta_0 = 5.3$) and five slit widths $D = 29$, 19, 11, 7, and 5. Again the choice of parameters was made on the basis of Cifra's MC data. The overall trends in Figure 5 are the same as in Figure 4. The difference is that K is smaller than in a good solvent. The reason is obvious: the osmotic pressure in a Θ solvent is lower than in a good solvent so the driving force for entering the pores is less. An equivalent statement is that, due to the lower osmotic pressure, the depletion thickness δ remains higher (see Figure 2). As a consequence, narrow pores ($D = 7$, 5) remain (nearly) empty over a wider concentration range than in a good solvent.

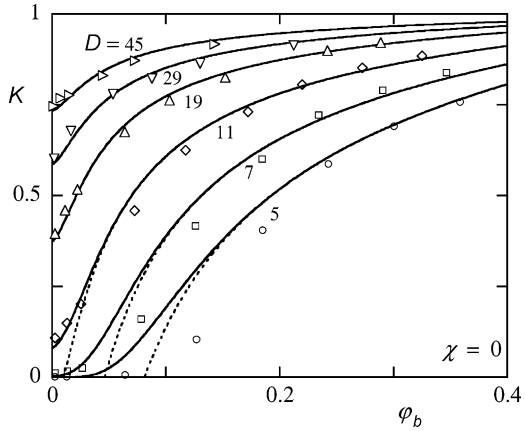

Figure 6. Monte Carlo results by Cifra et al. (open symbols) for the partition coefficient $K(\varphi_b)$ of self-avoiding chains with chain length $N = 100$ in an athermal solvent ($\chi = 0$), for six slit widths D (indicated). The solid curves were calculated from the modified Casassa equation (eq 3.2), and the dotted curves for $D = 5$, 7, and 11 are the extrapolation of the wide-pore equation $K = 1 - 2\delta/D$. The quantity δ was obtained from eq 5.1 (with $a = 0.44$) for ξ, in combination with eq 5.2 (with $\delta_0 = 6$ and $b = 0.6\varphi_b$).

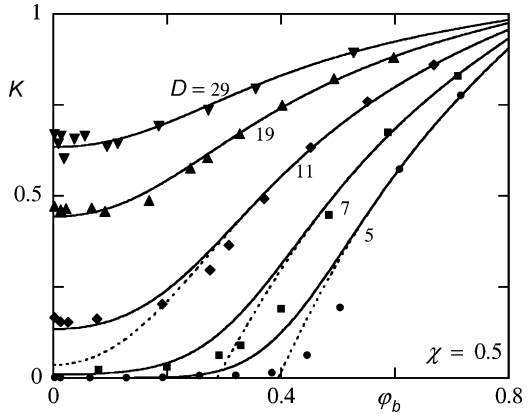

Figure 7. Monte Carlo results by Cifra et al. (filled symbols) for the partition coefficient $K(\varphi_b)$ of self-avoiding chains with chain length $N = 100$ in a Θ solvent ($\chi = 0.5$), for five slit widths D (indicated). The solid curves were calculated from the modified Casassa equation (eq 3.2), and the dotted curves for $D = 5$, 7, and 11 are the extrapolation of the wide-pore equation $K = 1 - 2\delta/D$. The quantity δ was obtained from eq 5.3 (with $a = 1.35$) for ξ, in combination with eq 5.2 (with $\delta_0 = 5.3$ and $b = 1.26$).

Again the solid curves in Figure 5 represent the modified Casassa equation (eq 3.2), and the dotted curves are the extrapolation of its wide-pore part $K = 1 - 2\delta/D$; in both cases eq 2.4 was used for δ. For $D = 29$, 19, and 11 the agreement between the analytical model and the numerical data is of the same level as in Figure 4. Only for $D = 7$ and 5 are some deviations visible, especially for low K; the overestimation of the numerical data is stronger. Nevertheless, the same conclusion can be drawn as in Figure 4; the combination of the single-wall depletion thickness δ (eq 2.4) with the modified Casassa equation (eq 3.2) or its wide-pore limit $K = 1 - 2\delta/D$ describes the partitioning data for high K excellently and the trends for lower K quite reasonably.

5. Partition Coefficient for MC Chains

5.1. MC Simulations. Figure 6 (open symbols) gives MC results as reported by Cifra et al.[11,50] for self-avoiding walks on a lattice. The partition coefficient K is plotted as a function of concentration for $N = 100$ and an athermal solvent, for six slit widths $D = 45$, 29, 19, 11, 7, and 5 (from top to bottom). These widths are one lower than reported by Cifra et al. because we want to mimic the boundary condition of zero concentration at the pore walls. In the simulations the segment−wall repulsion was taken to be infinitely high, resulting in two empty layers adjoining the walls. We translate that as $\varphi(0.5) = 0$ and $\varphi(D' - 0.5) = 0$, where D' is the slit width as reported by Cifra. By eliminating two half-layers from the system, $D = D' - 1$, we expect to be closer to the desired boundary condition $\varphi(0) = \varphi(D) = 0$.

Comparison of Figure 6 (MC chains) with Figure 4 (MF chains) shows that the qualitative aspects are essentially the same. However, there is a quantitative difference along the concentration scale: MC chains are excluded from narrow pores up to higher concentrations than MF chains. For example, for $D = 5$ in Figure 4 the slit is (nearly) empty below $\varphi_b \approx 0.05$ and in Figure 6 below $\varphi_b \approx 0.10$. The reason is that for MC chains the correlation length ξ scales differently with concentration as compared to MF chains; we discuss this point in section 5.3.

The curves in Figure 6 are based on extracting the single-wall depletion thickness $\delta(\varphi_b)$ from the wide-pore data ($K > 0.5$), using $\delta = (D/2)(1 - K)$. As will be shown below (Figures 8 and 9), $\delta(\varphi_b)$ does not depend on the slit width; for each solvency a single master curve is obtained which can be described by eqs 5.1 and 5.2. The solid curves in Figure 6 were computed by inserting this $\delta(\varphi_b)$ into our modified Casassa equation. The dotted curves are again the wide-pore limit $K = 1 - 2\delta(\varphi_b)/D$.

In Figure 7 we present the MC results[11,50] for a Θ solvent (filled symbols). Also here the curves were obtained from the wide-pore data, using eqs 5.2 and 5.3 for δ in combination with the modified Casassa equation (eq 3.2). As in the MF case (Figures 4 and 5), in a Θ solvent K is smaller than in a good solvent because the driving force (the osmotic pressure) for entering the pores is lower. Also for a Θ solvent MF chains enter the pores at a lower concentration than MC chains.

5.2. The Depletion Thickness for MC Chains. For the wide-pore regime ($K > 0.5$) where the depletion layers do not overlap we may extract the single-wall depletion thickness δ from the simulation data through $\delta = (D/2)(1 - K)$. Figures 8 and 9 (symbols) show $\delta(\varphi_b)$ obtained in this way for *all* the data in Figures 6 and 7 with $K > 0.5$. Open symbols are the good solvent results, and closed symbols are for a Θ solvent. In Figure 8 the concentration scale is linear, and in Figure 9 it is logarithmic.The most important conclusion is that for each solvency we obtain one master curve: all data for different D collapse onto one curve. This supports the notion that δ is a single-wall property, which is also relevant for a slit as long as the two depletion layers do not overlap (see Figure 1). In passing, we note that this universal behavior is only found when D and not $D' = D + 1$ is used to calculate δ. When δ is computed as $\delta = (D'/2)(1 - K)$, the data for $D' = 6$ and $D = 5$ deviate from the universal curve. This forms a justification of our choice for D.

The symbols in Figures 8 and 9 give the dependence $\delta(\varphi_b)$ for MC chains in a discrete form. A continuous dependence may be found by interpolating in some way or another between the data points. The curves in these figures may be seen as such an interpolation; they were obtained from eqs 5.1−5.3 in the next section. With this

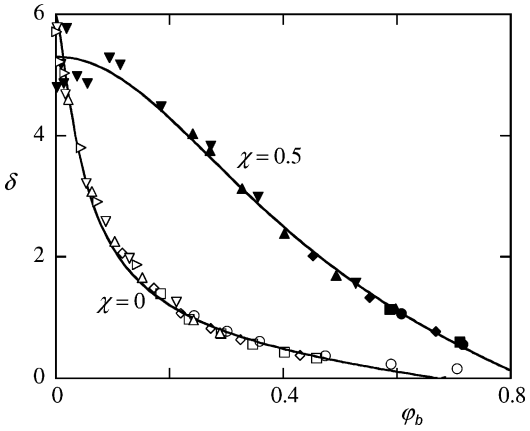

Figure 8. Depletion thickness $\delta(\varphi_b)$ as derived from the MC wide-pore data in Figures 6 and 7. The symbols were obtained from the numerical data points with $K > 0.5$ as $\delta = (D/2)(1 - K)$. The meaning of the symbols is the same as in Figures 6 and 7: open symbols $\chi = 0$, filled symbols $\chi = 0.5$, circles $D = 5$, squares $D = 7$, diamonds $D = 11$, triangles up $D = 19$, triangles down $D = 29$, triangles right $D = 45$. The solid curve for $\chi = 0$ was calculated from eqs 5.1 and 5.2 (with $\delta_0 = 6$, $a = 0.44$, and $b = 0.6\varphi_b$) and that for $\chi = 0.5$ from eqs 5.2 and 5.3 (with $\delta_0 = 5.3$, $a = 1.35$, and $b = 1.26$).

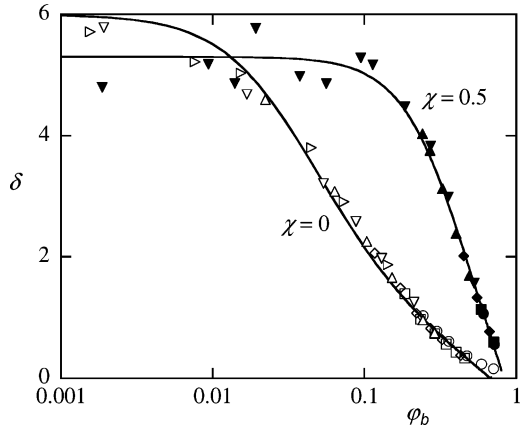

Figure 9. As Figure 8, but now with a logarithmic scale for $\delta(\varphi_b)$ to highlight the dilute regime.

$\delta(\varphi_b)$ dependence, the partition coefficient $K(\varphi_b)$ may be computed also for narrow pores using the modified Casassa equation (eq 3.2) with δ instead of δ_0. This is how the solid curves in Figures 6 and 7 were obtained. They describe the wide-pore data excellently, which is to be expected. However, they also indicate the trends in the narrow-pore regime quite reasonably. The data points for small K in narrow pores lie below the "modified Casassa curves", but not very much so. We note that the curves which extrapolate the wide-pore dependence $K = 1 - 2\delta/D$ all the way to $K = 0$ (dashed curves in Figures 6 and 7) follow the data points in narrow pores even better than the solid curves.

So, our second conclusion is that, in addition to the universal wide-pore behavior of MC chains, the trends in the narrow-pore regime may be reasonably described by using the depletion thickness as obtained only from wide-pore data ($K > 0.5$). In section 7 we shall consider the deviations in narrow pores in more detail.

5.3. Analytical Form for the MC Depletion Thickness. The last question concerning Figures 8 and 9 is whether we can find a functional form for the dependence $\delta(\varphi_b)$ for MC chains. Our starting point is eq 2.4, $1/\delta^2 = 1/\delta_0^2 + 1/\xi^2$ for a good solvent, but we allow for a scaling behavior $\xi(\varphi_b)$ which in good solvents is different from that for MF chains. Moreover, we correct for the fact that in the MC simulations the bounday condition $\varphi(0) = 0$ at the wall may not be satisfied.

Comparison of the data in Figure 8 with those in Figure 2 shows that in dilute solutions δ_{MC} for MC chains decays more gradually with φ_b than δ_{MF} for MF chains, whereas in (very) concentrated solutions δ_{MC} is somewhat lower than δ_{MF}; in the latter case the difference is less than half a bond length. The former effect is related to a different dependence of ξ on φ_b, and the latter is probably due to the boundary condition at the wall.

Athermal Solvent. In MF athermal solvents ($\chi = 0$), the correlation length $\xi = [-3 \ln(1 - \varphi_b)]^{-1/2}$ scales as $\varphi_b^{-1/2}$ (see eq 2.5). It is well known[45] that for chains with excluded-volume correlations the proper scaling in semidilute solutions is $\xi \propto \varphi_b^{-3/4}$. In (very) concentrated systems, where $\delta \approx \xi$ approaches zero, this scaling behavior breaks down. That is why we tentatively use

$$\xi = a[-\ln(1 - \varphi_b)]^{-3/4} \tag{5.1}$$

which not only reduces to the De Gennes' result $\xi \propto \varphi_b^{-3/4}$ in semidilute solutions but also gives the correct limit $\xi \to 0$, $\delta \to 0$ in the polymer melt. The prefactor a does not follow from a scaling analysis. When we modify eq 2.5 only with respect to the exponent and retain the factor 3, its value would be $a = 3^{-3/4} = 0.44$. Although we have no strict justification for this numerical value, $a = 0.44$ works adequately, as shown below.

Figure 9 (open symbols) shows that a fair estimate for the depletion thickness in the dilute limit is $\delta_0 = 6$. It turns out that $1/\delta^2 = 1/\delta_0^2 + 1/\xi^2$ with ξ given by eq 5.1 describes the good-solvent data in Figures 8 and 9 rather accurately, though not perfectly. We assume that the small remaining deviation is due to the boundary condition at the wall. Our eq 2.4 is based upon $\varphi(0) = 0$ at the pore wall. In the SCF computations this condition could be mimicked by tuning the segment–wall repulsion (see eq 2.7). In the MC simulations that is not so easy, and the profile extrapolates to $\varphi(b) = 0$, where b is some shift which is related to what Cifra et al. call the "penetration depth". We adopt an empirical approach, and we use eq 2.4 with ξ replaced by $\xi - b$:

$$\frac{1}{\delta^2} = \frac{1}{\delta_0^2} + \frac{1}{(\xi - b)^2} \tag{5.2}$$

Here ξ is given by eq 5.1, and b is an adjustable parameter which is obtained by fitting to Cifra's data; it may depend on φ_b as is also the case in the MF boundary condition of eq 2.7. It turns out that for an athermal solvent $b = 0.6\varphi_b$ (giving an offset varying from 0 in dilute solutions to 0.24 for $\varphi_b = 0.4$) gives a very nice description of the good-solvent data in Figures 8 and 9, as shown by the solid curves for $\chi = 0$ in these figures. Clearly, this empirical correction should be refined for very concentrated solutions, as it would lead to $\delta \approx b$ (instead of $\delta = 0$) in the melt.

Θ Solvent. In MF Θ solvents ($\chi = 0.5$), the correlation length is given by $\xi = [-3 \ln(1 - \varphi_b) - 3\varphi_b]^{-1/2}$; in semidilute solutions it scales as $\xi \propto \varphi_b^{-1}$, which also follows from scaling theory.[45] To get the correct limit $\xi = 0$ in the melt, we maintain again the logarithmic form of eq 2.5 and rewrite ξ as

$$\xi = a[-\ln(1 - \varphi_b) - \varphi_b]^{-1/2} \quad (5.3)$$

Again, a is a proportionality constant which in the strict mean-field version of eq 2.5 would be equal to $a = 3^{-1/2} = 0.58$. We will see below that the fit to the MC simulations requires a higher value $a = 1.35$. For the moment, it is not clear what the physical meaning of this constant is.

When inserting eq 5.3 into eq 5.2 to calculate δ, we also need the parameters δ_0 and b. From the filled symbols in the dilute regime of Figure 9 (which show some scatter) we see that a reasonable choice is $\delta_0 = 5.3$, slightly lower than in a good solvent, as expected. For the offset b a constant (concentration-independent) value suffices. The fit shown by the solid curves in Figures 8 and 9 corresponds to $b = 1.26$. Apparently, we need a higher offset than for an athermal solvent.

We repeat that the physical meaning of the constants a and b in eqs 5.1−5.3 is not quite clear, and we obtained their values by treating them as adjustable parameters. Nevertheless, the final result is rather satisfactory: the curves in Figures 8 and 9 describe the simulation data quite well over the concentration range shown. It would be interesting to see to what extent these constants depend on the chain length; at the moment we do not have data to analyze this dependence.

The overall conclusion of sections 5.1−5.3 is that we can extract from the simulation data for MC chains one master curve for the single-wall depletion thickness $\delta(\varphi_b)$ for each solvency, we can describe its functional form with an adjusted MF equation (eqs 5.1−5.3), and in combination with the modified Casassa equation we can also interpret the trends in the narrow-pore behavior (low K) in the original simulation data. As in the MF case, we find that in the narrow-pore regime the modified Casassa equation overestimates the partition coefficient somewhat.

6. Master Plots for MF and MC Chains

In the previous section we have seen that the modified Casassa equation (eq 3.2) describes $K(\varphi_b)$ quite well over a wide range of K, both for the MF results and for the MC simulations and both for athermal and Θ solvents. Only for low K in narrow pores does this equation overestimate the numerical MF and MC data. We deal with this issue in the next section. Disregarding this overestimation for the moment, we can use eq 3.2 to construct one "modified Casassa plot", of the type of Figure 3 but now with $2\delta/D$ along the abscissa axis instead of $2\delta_0/D$. To be able to do so, we have to convert the concentration scale in Figures 4−7 to δ. For the MF data we can apply eq 2.4, and for the MC simulations we can use eqs 5.1−5.3 with the appropriate constants for both solvencies.

When such a plot is made for the MF data of Figures 4 and 5 with eq 2.4 for the conversion, we do obtain quite a good master curve in the wide-pore region which, however, shows some scatter (of the same order of magnitude as in Figure 11). The reason for this scatter is that eq 2.4, even though it works quite well, is nevertheless only an approximation. In this case we have an alternative by using not eq 2.4, but the numerically exact δ values calculated from the upper curves (widest slit) in Figures 4 and 5 as $\delta = (D/2)(1 - K)$. To illustrate the principle, we use the latter procedure here.

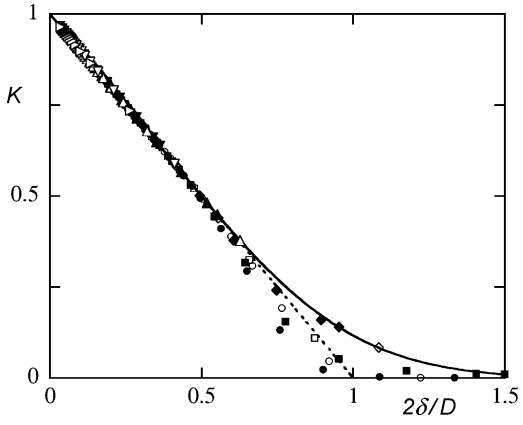

Figure 10. Modified Casassa plot for all the SCF data of Figures 4 and 5. The depletion thickness δ was calculated as $\delta = (D/2)(1 - K)$ for the widest slit ($D = 45$ for $\chi = 0$ and $D = 29$ for $\chi = 0.5$). The symbols are the same as in Figures 4 and 5: open symbols $\chi = 0$, filled symbols $\chi = 0.5$, circles $D = 5$, squares $D = 7$, diamonds $D = 11$, triangles up $D = 19$, triangles down $D = 29$, triangles right $D = 45$. The solid curve is the modified Casassa equation (eq 3.2), and the dotted line is the extrapolation of its wide-pore limit.

Figure 10 shows the results obtained by plotting *all* the numerical SCF data of Figure 4 (athermal) and Figure 5 (Θ) in this way. The solid curve in this figure is the modified Casassa equation (eq 3.2). In the wide-pore regime ($K > 0.5$) a perfect (linear) master curve is obtained. In the narrow-pore regime, the data for $D = 11$ and low concentration (where $\delta \approx \delta_0$) follow the "narrow" part of the Casassa curve nicely, but for $D = 5$ and 7 we see the same overestimation in the narrow-pore regime as in Figures 4 and 5. The deviations for a Θ solvent are higher than for a good solvent as was also seen in Figures 4 and 5.

Nevertheless, it is gratifying to note that the widely different curves of Figures 4 and 5 for two solvencies largely collapse onto one universal curve. Only for narrow pores and intermediate concentrations ($2\delta/D > 0.5$) is this universality lost. In this region the master curve gives an upper bound for K: all deviations are in the downward direction. The reason for these deviations will be discussed in the next section.

Figure 11 shows the same plot for the MC simulations. Here we used eqs 5.1−5.3 for the conversion from φ_b to δ. Again, Figure 11 contains all the data from Figures 6 and 7. This figure for the MC simulations is nearly identical to Figure 10 for the MF computations. The same universal behavior is found for the wide-pore regime and for relatively dilute systems for $D = 11$, and the same nonuniversal effects (again in the downward direction) occur for narrow pores ($D = 5$, 7) and intermediate concentrations. Also for MC chains the deviations are strongest in a Θ solvent. Even quantitatively Figures 10 and 11 are nearly the same.

In the following section we consider the nonuniversal aspects in narrow pores.

7. The Narrow-Pore Regime at Finite Concentrations

From Figure 1b it is clear that the appropriate length scale in the wide-pore regime (where the depletion layers do not overlap) is the single-wall depletion thickness δ. It leads to $K = 1 - 2\delta/D$ for the wide-pore regime and to the universal linear part in Figures 10 and 11.

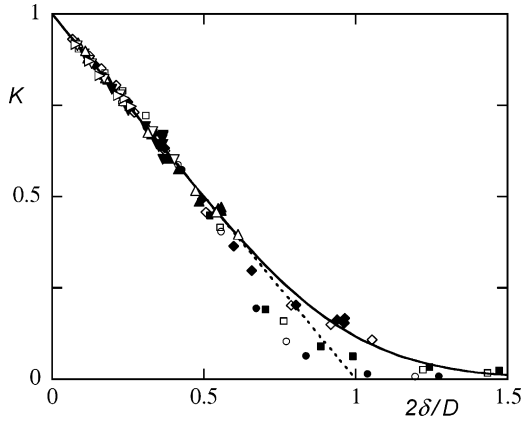

Figure 11. Modified Casassa plot for all the MC data of Figures 6 and 7. The symbols are the same as in Figure 10. The depletion thickness δ for $\chi = 0$ was calculated from eqs 5.1 and 5.2 (with $\delta_0 = 6$, $a = 0.44$, and $b = 0.6\varphi_b$) and that for $\chi = 0.5$ from eqs 5.2 and 5.3 (with $\delta_0 = 5.3$, $a = 1.35$, and $b = 1.26$). The solid curve is the modified Casassa equation (eq 3.2), and the dotted line is the extrapolation of its wide-pore limit.

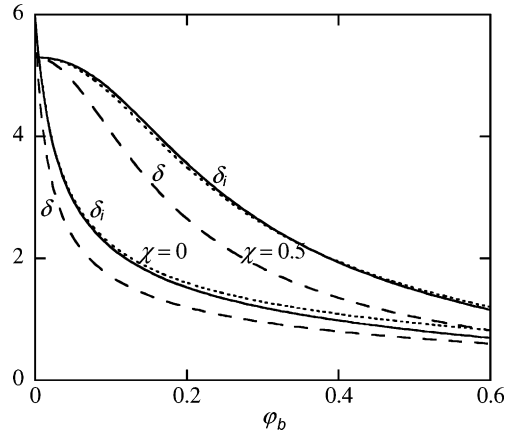

Figure 12. Interaction distance $\delta_i(\varphi_b)$ for the conditions of Figure 2, both with the full eq A6 (solid) and the expanded form of eq 7.1 (dotted). For comparison, $\delta(\varphi_b)$ is also plotted as the dashed curves (the same as the solid curves in Figure 2).

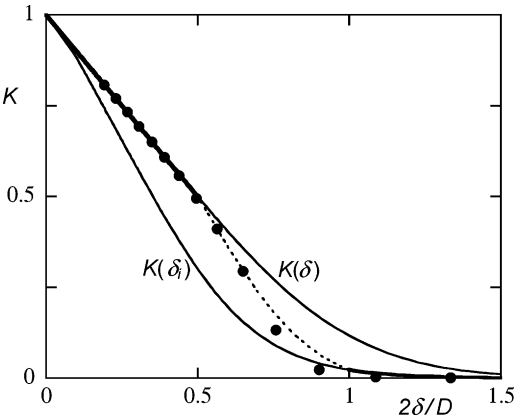

Figure 13. Interpolation between $K(\delta)$ and $K(\delta_i)$ according to eq 7.2, for $D = 5$ and $\delta_0 = 5.3$ in a Θ solvent. Both $K(\delta)$ and $K(\delta_i)$ were calculated from the modified Casassa equation (eq 3.2) with, however, a different length scale: δ according to eq 2.4 and δ_i from eq 7.1 (or eq A6). The dotted curve interpolates according to eq 7.2 between the thick curves, which are the wide-pore part of $K(\delta)$ and the narrow-pore part of $K(\delta_i)$. The symbols are SCF results and are the same as the filled circles in Figure 10.

In the narrow-pore regime the two depletion layers do overlap. Now it is not obvious that the same length scale δ is the relevant one. In fact, we will show below that a different length scale δ_i, which may be called the interaction distance, is needed. For dilute systems $\delta_i = \delta = \delta_0$ but in semidilute solutions $\delta_i > \delta$, the more so in a Θ solvent. As a consequence, K in narrow pores is smaller than given by the modified Casassa equation using only δ.

Information about the value of δ_i in narrow pores can be obtained from considering the pair potential $W(D)$ between two flat plates in a solution of nonadsorbing polymer. Some more background is given in the appendix, based upon two recent papers by Tuinier and Fleer.[47] The essential point is that in nearly empty slits $W(D)$ is linear in D, $W(D) = \Pi(D - 2\delta_i)$, where Π is the osmotic pressure of the bulk solution and δ_i is the interaction distance. In dilute solutions where an exact solution[51] for $W(D)$ is available (eq A1), δ_i equals δ_0 as defined in eq 2.3; for dilute solutions there is only one length scale for both the wide- and narrow-pore regimes. For semidilute solutions δ_i is in between the single-wall depletion thickness δ and δ_0; now the length scales for the two regimes are different. The ratio δ_i/δ is approximately given by[47]

$$\frac{\delta_i}{\delta} \approx \frac{1/N + (2/3)v\varphi_b + (1/2)\varphi_b^2}{1/N + (1/2)v\varphi_b + (1/3)\varphi_b^2} \qquad (7.1)$$

A more precise definition of δ_i is presented in eq A6. From eq 7.1 it follows that in the dilute limit $\delta_i = \delta$ $(=\delta_0)$. When the linear concentration terms dominate, as for semidilute concentrations in a good solvent, $\delta_i/\delta = 4/3$, and in semidilute Θ solutions $\delta_i/\delta = 3/2$ for large N. A plot of the interaction length $\delta_i(\varphi_b)$ as compared to the depletion thickness $\delta(\varphi_b)$ for the conditions of Figure 2 is given in Figure 12, with for δ_i both the approximate form of eq 7.1 (dotted curves) and the more accurate eq A6 (solid). The dashed curves in Figure 12 represent $\delta(\varphi_b)$ and are the same as the solid curves in Figure 2; they are below δ_i, as expected from eq 7.1.

So we have obtained a new length scale δ_i for narrow slits. In the spirit of our present approach, it is reasonable to apply the modified Casassa equation for nearly empty slits (say, for $2\delta/D > 1$) with δ_i instead of δ as the length scale. Comparison with the exact SCF results shows good agreement. Although δ_i/δ is not much above unity (its maximum value is 3/2 for a Θ solvent), the effect on K is considerable because the square of δ_i/D occurs in the exponent. This is shown in Figure 13 by the curves $K(\delta)$ (eq 3.2 with δ) and $K(\delta_i)$ (eq 3.2 with δ_i). This figure was computed for $\chi = 0.5$, $\delta_0 = 5.3$, and $D = 5$, using eq 2.4 for δ and eq A6 for δ_i, over a wide concentration range. The SCF results, taken from Figure 10, are also indicated. The wide-pore section of $K(\delta)$ is linear because K is plotted against $2\delta/D$, and that of $K(\delta_i)$ is not linear because δ_i/δ depends on φ_b (it would become linear when plotted against $2\delta_i/D$).

We have now two obvious limits: $K = 1 - 2\delta/D$ for wide pores ($2\delta/D < 0.5$), with length scale δ, and $K = (8/\pi^2)\exp[-\pi^3(\delta_i/2D)^2]$ for narrow pores ($2\delta/D > 1$), with a slightly larger length scale δ_i. This small difference gives rise to a significantly lower K: $K(\delta_i) < K(\delta)$, as shown in Figure 13. These two limits are indicated in Figure 13 by the thick curves.

In Figure 13 we see that in the intermediate region ($0.5 < 2\delta/D < 1$) the numerical data smoothly cross over

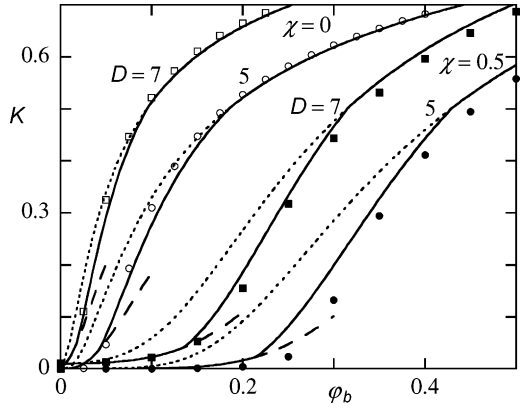

Figure 14. Narrow-pore data ($D = 5$ and 7) of Figures 4 and 5. Symbols as in Figures 4 and 5. The dotted curves are $K(\delta)$ and are the same as the solid curves Figures 4 and 5. The dashed curves represent $K(\delta_i)$ with δ_i from eq 7.1. The solid curves were computed with the interpolation according to eq 7.2.

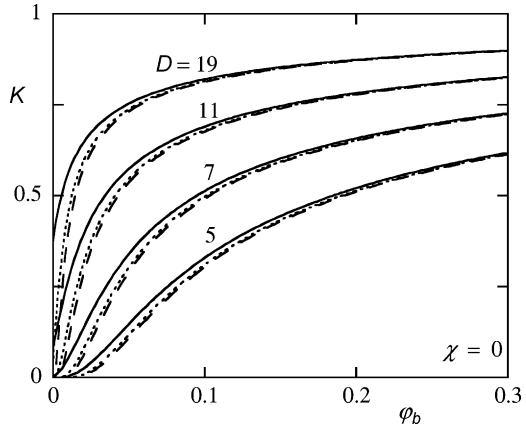

Figure 15. Effect of the chain length on the distribution coefficient $K(\varphi_b)$ in a good solvent ($\chi = 0$), for four slit withs D as indicated. Solid curves $\delta_0 = 6$, dotted curves $\delta_0 = 12$, dashed curves $\delta_0 = \infty$.

from one limit to the other. It is a very difficult problem to analytically describe this crossover from first principles. However, we can adopt an empirical approach and interpolate between $K(\delta)$ and $K(\delta_i)$ by using a linear combination of the form $K = (1 - y)K(\delta) + yK(\delta_i)$, where the parameter y is linear in $2\delta/D$ and takes the values $y = 0$ at $2\delta/D = 0.5$ and $y = 1$ at $2\delta/D = 1$. Then $y = 4\delta/D - 1$, and we find the following approximation for K:

$$K = \begin{cases} 1 - \dfrac{2\delta}{D} & \dfrac{2\delta}{D} < 0.5 \\ \dfrac{8}{\pi^2}\left\{\left(2 - \dfrac{4\delta}{D}\right)e^{-\pi^3(\delta/2D)^2} + \left(\dfrac{4\delta}{D} - 1\right)e^{-\pi^3(\delta_i/2D)^2}\right\} & 0.5 < \dfrac{2\delta}{D} < 1 \\ \dfrac{8}{\pi^2}\, e^{-\pi^3(\delta_i/2D)^2} & \dfrac{2\delta}{D} > 1 \end{cases} \tag{7.2}$$

The dotted curve in Figure 13 is calculated with eq 7.2b; it gives a fair (though obviously not precise) description of the SCF data. Since the averaging procedure of eq 7.2b leads to a result which in the transition region is rather close to the extrapolated wide-pore equation, we can now also understand why in Figures 4−7 this extrapolation describes the numerical partition coefficients fairly well. We note that an interpolation equation of the type $\delta_{int} = (1 - y)\delta + y\delta_i$, with K calculated from eq 3.2 after replacing δ by this interpolation distance δ_{int}, gives nearly identical results (not shown) as interpolating K according to eq 7.2b.

We can now reinterpret the narrow-pore curves in Figures 4 and 5. Figure 14 shows the data for $D = 5$ and 7 from these two figures (in a slightly enlarged version). The symbols are the same SCF results as in Figures 4 and 5. The dotted curves are the original $K(\delta)$ and are the same as the solid curves in Figures 4 and 5. The dashed curves give $K(\delta_i)$; they lie considerably below $K(\delta)$ since $\delta_i > \delta$. The solid curves in Figure 14 are drawn according to eq 7.2. In all cases the interpolation formula eq 7.2b gives a fair description of the SCF data. That is all we may expect for such a rough interpolation.

In principle, we could follow the same procedure for the MC simulations in the transition region of Figures 6 and 7. We will not do that here, as we do not know whether the ratio δ_i/δ as given in eq 7.1 (or eq A6), which is a strict mean-field result, is also valid for MC chains. However, the fact that the modified Casassa plots in Figure 10 (MF) and Figure 11 (MC) are nearly the same, even quantitatively, suggests that a relation of the type of eq 7.1 would also work for MC chains.

Finally, we note that we now have two length scales, δ for wide pores and δ_i for narrow ones (and both δ and δ_i in the transition region). Since the ratio δ_i/δ is not a constant, modified Casassa plots as in Figures 10 and 11, K vs $2\delta/D$, are no longer universal for $2\delta/D > 0.5$. These nonuniversal features are clearly seen in Figures 10 and 11. We could make the narrow-pore region universal by plotting against $2\delta_i/D$, but then the universality in the wide-pore region is lost, so we will not do that. For the transition region, where both length scales play a role, we have to accept inherent nonuniversal features, which cause K to be lower than given by the "universal" modified Casassa equation using only δ.

8. Effects of Chain Length, Solvency, and Chain Stiffness

So far we have discussed only results for one fixed chain length and two solvencies ($\chi = 0$ and 0.5) since we used the MC simulations by Cifra et al.[11,50] as the reference point. In this final section we consider the effects of the chain length N (or the value $\delta_0 = (2N/3\pi)^{1/2}$ of the depletion thickness in the dilute limit), the effect of intermediate solvencies, and that of chain stiffness. We base ourselves on the "universal" mean-field description as given by the modified Casassa equation (eq 3.2), using only the wide-pore length scale (depletion thickness) δ as given by eq 2.4. From the previous section we know that this simple treatment overestimates K in the narrow-pore regime. However, we expect that the trends are correctly described and that these trends are not only valid for MF chains but also for real (self-avoiding) chains.

8.1. Chain Length. Figure 15 presents $K(\varphi_b)$ for four slit widths ($D = 19$, 11, 7, and 5 from top to bottom) and three values of δ_0: 6 (solid curves), 12 (dotted), and ∞ (dashed), in a good solvent. The solid curves for $\delta_0 = 6$ are the same as in Figure 4. Increasing the chain length has hardly any effect in semidilute solutions where the term $1/\delta_0^2$ in eq 2.4 is small so that $\delta \approx \xi$. The dotted curves for $\delta_0 = 12$ nearly coincide with the infinite-chain limit $\delta_0 = \infty$ (dashed). In this semidilute

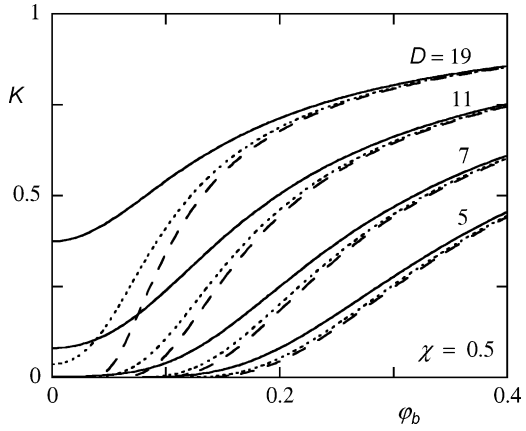

Figure 16. Effect of the chain length on the distribution coefficient $K(\varphi_b)$ in a Θ solvent ($\chi = 0.5$), for four slit withs D as indicated. Solid curves $\delta_0 = 6$, dotted curves $\delta_0 = 12$, dashed curves $\delta_0 = \infty$.

regime K is thus essentially only a function of the concentration according to

$$K = \begin{cases} 1 - \dfrac{2\xi}{D} & 2\xi/D < 0.5 \\ \dfrac{8}{\pi^2} e^{-\pi^3(\xi/2D)^2} & 2\xi/D > 0.5 \end{cases} \qquad (8.1)$$

where $\xi = [-3 \ln(1 - \varphi_b)]^{-1/2} \approx (3\varphi_b)^{-1/2}$ for $\chi = 0$. In this regime there is no chain-length dependence, and separation on the basis of chain length is impossible.

Only in the (very) dilute regime and for relatively wide pores ($D = 19$ and 11) is the partition coefficient still a function of the chain length, with a higher K for shorter chains. However, in narrow pores ($D = 7$ and 5) this chain-length dependence is nearly absent even in very dilute solutions, as can be seen by comparing the solid and dashed curves for the two lowest slit widths in Figure 15. For long chains in dilute solutions K is close to zero in narrow pores, so again no separation on the basis of chain length is possible. The only regime where such a separation is feasible in a good solvent is for dilute solutions, relatively short chains, and wide pores.

Figure 16 shows similar data for a Θ solvent. Although in principle the same effects occur, the chain-length dependence is maintained much longer, especially in wide pores. For high concentrations eq 8.1 still holds, provided ξ is replaced by $\delta = p\xi$ with $p = 0.81$, and in this case $\xi = [-3 \ln(1 - \varphi_b) - 3\varphi_b]^{-1/2} \approx (2/3)^{1/2}\varphi_b^{-1}$, but the validity of this equation is limited to a narrower concentration regime. The reason is that the term $1/\delta_0^2$ in eq 2.4 is relatively more important: it has to be balanced against the φ_b^2 term in the expansion of ξ^{-2} (eq 2.5), whereas in good solvents this balancing is against the (higher) linear φ_b term. Therefore, in a Θ solvent the separation on the basis of chain length is easier than in a good solvent. This has also been found experimentally.[17]

8.2. Solvency. Figures 15 and 16 demonstrate again, as seen before (Figures 4−7), that the distribution coefficient in a Θ solvent ($\chi = 0.5$) is smaller than for $\chi = 0$. Figure 17 illustrates the effect of solvency in the intermediate region for χ. We restrict ourselves to $0 < \chi < 0.45$, where the parameter p in eq 2.4 may be taken as unity. We do know the value of p (0.81) in a Θ solvent, but not so for the solvency range $0.45 < \chi < 0.5$, where

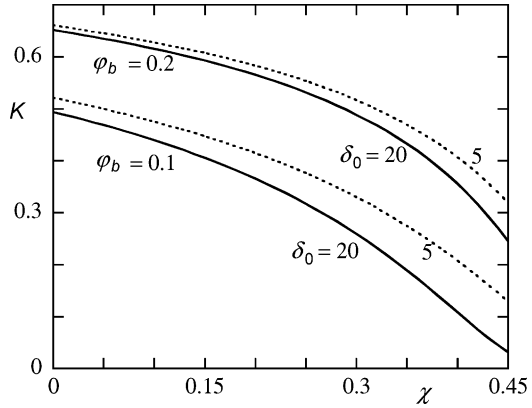

Figure 17. Distribution coefficient K in a slit of width $D = 7$ as a function of solvency χ, for $\varphi_b = 0.1$ (lower curves) and 0.2 (upper curves), and $\delta_0 = 5$ (dotted) and 20 (solid).

our model is inaccurate as we have no easy description of the crossover $p(\chi)$ from the value 1 in good solvents to 0.81 in a Θ solvent. Since we only want to describe trends, the range $0 < \chi < 0.45$ or $1 > \upsilon > 0.1$ is adequate: in this region $\xi \approx (3\upsilon\varphi_b)^{-1/2}$ for not too high φ_b. For $\varphi_b = 0.1$, ξ increases from 1.83 for $\chi = 0$ to 2.89 for $\chi = 0.3$ to 5.78 for $\chi = 0.45$. For $\varphi_b = 0.2$, these numbers are smaller by a factor $\sqrt{2}$: 1.29 for $\chi = 0$, 2.04 for $\chi = 0.3$, and 4.08 for $\chi = 0.45$.

In Figure 17, which applies to $D = 7$, $\varphi_b = 0.1$ and 0.2, and $\delta_0 = 5$ and 20, we see that K decreases gradually with χ. The curves for $\delta_0 = 20$ nearly coincide with the high-N limit (not shown), and they are therefore described by eq 8.1 with $\xi \approx (3\upsilon\varphi_b)^{-1/2}$ and numbers for ξ as given above. The decrease of K with increasing χ is then essentially only due to the increasing ξ. As ξ is lower at higher concentrations (roughly by a factor of $\sqrt{2}$ in Figure 17), K increases with φ_b. The wide-pore data ($K > 0.5$) in Figure 17 follow $K = 1 - 2\xi/D$; for smaller K the decrease goes as $\exp[-\pi^3(D/2\xi)^2]$ and is therefore faster.

For $\delta_0 = 5$ in Figure 17, the term $1/\delta_0^2$ is not yet negligible with respect to $1/\xi^2$, and δ is smaller than ξ (see Figure 2) so that the curves for K lie above those for $\delta_0 = 20$. This effect is more noticeable for high χ (high ξ), where $1/\xi^2$ is smaller so that the effect of chain length is stronger than for low χ. This is fully in line with our conclusion above that separation on the basis of chain length is easier in a Θ solvent as compared to a good solvent.

The effect of solvency for MC chains was considered by Cifra at al.[11] using computer simulation. The trends are in full agreement with our MF theory.

8.3. Chain Stiffness. Finally, in Figure 18 we consider the effect of chain rigidity (persistence length). We incorporate this effect by redefining δ_0 in eq 2.3 as $\delta_0 = (2NA/3\pi)^{1/2}$, where A is a measure for the persistence length. Clearly, for flexible chains $A = 1$ and for stiff chains it is larger. It is obvious that by using this definition and applying eq 2.4 for δ the effect of the chain stiffness is the same as rescaling the chain length N.

Figure 18 gives an example for $N = 100$, $D = 12$, two values of A (1 and 2), and two solvencies χ (0 and 0.5). The trends in Figure 18 are thus the same as in Figures 15 and 16, where we discussed the chain-length dependency. We nevertheless show Figure 18 separately because it enables a comparison with MC simulations for stiff chains by Skrinarova and Cifra.[36,37] These

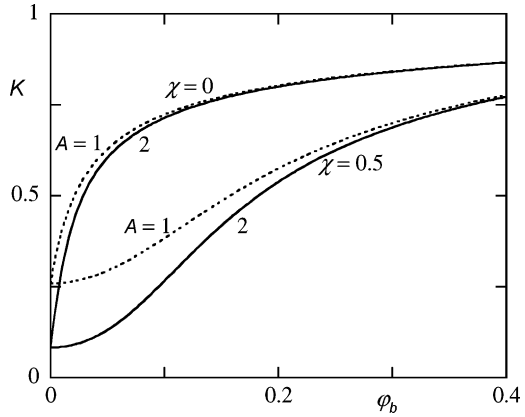

Figure 18. Effect of chain stiffness on the distribution coefficient $K(\varphi_b)$, for $N = 100$, $D = 12$, and $\chi = 0$ (upper curves) and $\chi = 0.5$ (lower curves). The curves for flexible chains ($A = 1$) are dotted, and those for stiffer chains ($A = 2$) are solid.

authors found that for $\chi = 0$ there is hardly any effect of the chain stiffness, whereas in a Θ solvent at low concentrations K is significantly lower for stiffer chains. For higher concentrations in a Θ solvent the effect of chain stiffness is smaller; the simulation data even suggest a crossover, with K for stiff chains at high concentrations slightly higher than for flexible ones.

Figure 18 shows essentially the same trends. Also here we see only a small effect of chain stiffness (chain length) for $\chi = 0$. The reason is that the $1/\delta_0^2$ term in eq 2.4 hardly contributes as it small with respect to $1/\xi^2 = 3\varphi_b$. In a Θ solvent the effect of chain stiffness (chain length) at low concentrations is stronger because $1/\xi^2 = (3/2)\varphi_b^2$ is much smaller. At high concentrations in a Θ solvent the value of $1/\xi^2$ is higher, and the precise value of δ_0 no longer matters, since $1/\delta_0^2$ becomes negligible: the curves for different A converge. Our simple model therefore explains the main trends. It does not capture the crossover at high concentrations in a Θ solvent as found by Skrinarova and Cifra.[37] This subtle effect may be related to the boundary condition at the wall: ideally we would like $\varphi(0) = 0$, but this is not easily accomplished in the MC simulations. In the actually achieved boundary condition $\varphi(b) = 0$, the penetration depth b may depend on chain stiffness.

9. Concluding Remarks

We presented a simple analytical equation for the distribution coefficient of polymers in size-exclusion chromatography (SEC) as a function of molar mass, concentration, and solvent quality. We based our theory on two ingredients.

The first is the universal relation between the distribution coefficient and the depletion thickness δ in wide pores: $K = 1 - \alpha\delta/D$, where D is the pore size and α a geometrical factor. For slitlike pores $\alpha = 2$. In general, α is determined by the ratio of the pore surface area to the pore volume, and δ depends on the chain architecture (linear, branched, or dendritic) and on concentration and solvency. When these factors are taken into account, the above relation is valid for arbitrary pore-size distribution and chain architecture. Hence, it is not based on some specific model for the polymer chain or the porous medium.

We note that in practical applications of SEC in dilute solutions the universal wide-pore regime with $D > 4R$ is more important than the narrow-pore regime (where such a universal relation does not exist). In concentrated solutions where $\delta \approx \xi$ is small, $K = 1 - 2\xi/D$ even for relatively small D: the wide-pore regime is relevant even in narrow pores. Consequently, almost all porous media in concentrated solutions can be considered as wide-pore media.

Our second ingredient is the relation between the single-wall depletion thickness δ and the properties of the polymer and the polymer solution. We exploit a general mean-field equation,[42] which for most solvency conditions reads $\delta^{-2} = \delta_0^{-2} + \xi^{-2}$. Here δ_0 is a polymer property; it is the depletion thickness at infinite dilution, which according to the classical theory[6,43,44] is somewhat higher than the radius of gyration R: $\delta_0 = (2/\sqrt{\pi})R$. The length ξ is a correlation length in solution, which is a solution property: it depends on concentration and solvency. As a result, a direct relation between the distribution coefficient K and the correlation length ξ is obtained. It even gives the possibility to measure ξ using SEC; we will discuss this aspect in a future publication in more detail.

To describe the concentration dependence $\xi(\varphi_b)$ and therefore the dependence $K(\varphi_b)$, we used mean-field theory for the polymer solution. Such a theory does not take into account the correlation of density fluctuations and as a result underestimates $\xi(\varphi_b)$ in a semidilute solution in a good solvent. In addition, a mean-field approach cannot describe the contraction of polymer chains with increasing concentration in a good solvent, from swollen to Θ conformations. This contraction is important in the semidilute region where the polymer concentration is of the order of the overlap concentration $\varphi_{ov} \approx Nl^3/R^3$. The reason why we nevertheless focus on a mean-field approach is that it enables us to make a comparison with exact numerical self-consistent-field (SCF) results; in this way we can check the assumptions that have to be made to obtain analytical approximations. Moreover, concentration effects are important not only in the semidilute regime but also in the marginal and concentrated regimes where the mean-field theory is correct.

So we first corroborated that our analytical approach is in accordance with numerical SCF data. In addition, we can also interpret the results of Monte Carlo (MC) simulations on self-avoiding chains. We found that the MC results in a slitlike pore follow the universal relation $K = 1 - 2\delta/D$ for wide pores ($K > 0.5$), where the depletion thickness δ does not depend on D because δ is a single-wall property. Therefore, the dependence $\delta(\varphi_b)$ may be directly extracted from the wide-pore data for K. We could describe this dependence in the MC simulations with our mean-field equation after adjusting the scaling exponent to $\xi \sim \varphi_b^{-3/4}$ in a good solvent. For a quantitative description, we need some corrections that are related to the boundary condition (penetration depth) at the wall.

We also considered the narrow-pore regime, where nonuniversal effects show up, both in the SCF results and for the MC data. In dilute solutions, where the original Casassa theory with one length scale δ_0 applies, these nonuniversal aspects are absent. We modified the Casassa equation by replacing δ_0 by δ and found that in this way an upper bound for the SCF and MC results is obtained: at finite concentrations the numerical results for K in the narrow-pore regime are systematically lower than predicted by this modified Casassa equation. The reason is that for interacting depletion layers a new length scale δ_i (the "interaction distance")

appears, which is somewhat larger than δ. Substituting this δ_i into the Casassa equation gives a good description for nearly empty pores (very low K). In the intermediate region an interpolation equation using both length scales can describe the numerical data quite reasonably.

The advantage of our approach is the simplicity of the analytical equations for a wide range of polymer concentrations. For example, we found that the equation $K = 1 - 2\delta/D$, which is accurate in the wide-pore regime ($2\delta/D < 0.5$), is also useful in the narrow-pore regime, where the simple form $K = 1 - 2\delta/D$ for $2\delta/D < 1$ and $K = 0$ for $2\delta/D > 1$ gives a reasonable first-order estimate for K in this regime. Because of this simplicity, our model opens the possibility to analyze the experimental data for the distribution coefficient in concentrated solutions and to develop a theory for the resolution in preparative SEC. It is even possible to describe analytically the interaction force (pair potential) between two surfaces in the presence of nonadsorbing polymer as a function of the concentration. We will discuss some of these issues in a later publication.

Acknowledgment. The authors thank Peter Cifra (Bratislava, Slowakia) for making available the numerical results of his computer simulations and for useful discussions. We gratefully acknowledge the discussions with Remco Tuinier (Jülich, Germany), especially about the product function approximation and the interaction distance. Support by the NWO Dutch-Russian Program "Computational Approaches for Polymers" and the INTAS Grant 2000-0031 enabled AMS to visit Wageningen, where most of this research was carried out.

Appendix. The Interaction Length δ_i

We briefly recapitulate the results for the pair potential $W(D)$ between two flat plates as obtained by Tuinier and Fleer.[47] For ideal chains in the dilute limit an exact result due to Asakura and Oosawa[51] is available, which we write as

$$W(D) = -\Pi[2\delta_0 - (1 - K_0)D] \qquad \Pi = \varphi_b/N \quad \text{(A1)}$$

Here, $W(D)$ is in units kT/l^2, and Π (in units kT/l^3) is the osmotic pressure; for ideal chains it is given by the Van't Hoff law $\Pi = \varphi_b/N$. The parameters δ_0 and K_0 are defined in eqs 2.3 and 3.1, respectively. For wide slits $(1 - K_0)D = 2\delta_0$ and $W(D) = 0$, as expected for nonoverlapping depletion layers.

For nearly empty slits ($1 - K_0 \approx 1$), $W(D)$ is linear in D:

$$W(D) = -\Pi(2\delta_0 - D) \qquad \frac{2\delta_0}{D} > 1.3 \qquad W(0) = -2\Pi\delta_0 \quad \text{(A2)}$$

Basically, this equation is equivalent to considering the pair potential in (nearly) empty slits to be described as the (outside) osmotic pressure Π times the overlap volume V_{ov} of the two depletion layers: $AW(D) = \Pi V_{ov}$, where A is the area per plate; in this case $V_{ov} = A(2\delta_0 - D)$, with δ_0 for overlapping depletion layers the same as the single-plate depletion thickness δ_0.

The exact calculations according to eq A1 show that the linear behavior of eq A2 is valid for $2\delta_0/D > 1.3$. An essential point of eqs A1 and A2 is that the same length scale δ_0 describes both the wide-pore and narrow-pore regimes.

Tuinier and Fleer[47] generalized eq A2 to finite concentrations. They concluded that eq A2 has to be modified in two aspects: a more general expression for Π is needed, and δ_0 has to be replaced by a length δ_i (the "interaction distance") which turns out to be close to the single-wall depletion thickness δ (eq 2.4) but in semidilute solutions is somewhat larger.

In a mean-field picture Π is given by the Flory–Huggins expression:[52]

$$\Pi = -\ln(1 - \varphi_b) - \varphi_b\left(1 - \frac{1}{N}\right) - \chi\varphi_b^2 = \frac{\varphi_b}{N} + \frac{1}{2}\upsilon\varphi_b^2 + \frac{1}{3}\varphi_b^3 + \ldots \quad \text{(A3)}$$

With this form of Π, eq A2 is modified to

$$W(D) = -\Pi(2\delta_i - D) \qquad \frac{2\delta_i}{D} > 1.3 \qquad W(0) = -2\Pi\delta_i \quad \text{(A4)}$$

We may still interpret this as $AW(D) = \Pi V_{ov}$, but now $V_{ov} = A(2\delta_i - D)$ and not $V_{ov} = A(2\delta - D)$. An expression for δ_i was derived by comparing the contact potential $W(0) = -2\Pi\delta_i$ with the exact expression

$$W(0) = -2\Omega \quad \text{(A5)}$$

where $\Omega \equiv \gamma - \gamma_0$ is the grand potential of a single plate in contact with a solution of nonabsorbing polymer. By definition, Ω is the difference between the surface free energy γ for the surface in contact with the polymer solution and γ_0 for the surface in contact with only solvent. By comparing eq A4b with eq A5, we find

$$\delta_i = \frac{\Omega}{\Pi} \qquad \frac{\delta_i}{\delta} = \frac{\Omega/\delta}{\Pi} \quad \text{(A6)}$$

which may be seen as the defining equation for the interaction length δ_i.

Exact results for the grand potential Ω are obtained from the numerical SCF lattice model. Tuinier and Fleer[47] also derived an analytical approximation which describes these exact results very well:

$$\frac{\Omega}{\delta} = \frac{2f}{9}\frac{\varphi_b}{\delta^2} \approx \frac{\varphi_b}{N} + \frac{2}{3}\upsilon\varphi_b^2 + \frac{1}{2}\varphi_b^3 \quad \text{(A7)}$$

The factor f, defined as $f = 1 - (1 - 3/\pi)\delta^2/\delta_0^2$, is nearly a constant; its value increases from $3/\pi = 0.955$ in the dilute limit ($\delta = \delta_0$) to 1 in semidilute solutions. By inserting eq A7b and the expanded form of Π (eq A3) into eq A6, eq 7.1 of the main text is obtained. In the dilute limit ($\Omega/\delta = \Pi = \varphi_b/N$), $\delta_i = \delta = \delta_0$, and eq A2 is recovered. For finite concentrations $\delta_i > \delta$, see eq 7.1, and the length scales δ for the wide-pore regime and δ_i for the narrow-pore limit are different.

References and Notes

(1) Yau, W. W.; Kirkland, J. J.; Bly, D. D. *Modern Size Exclusion Liquid Chromatography;* John Wiley: New York, 1979.
(2) Snyder, L. R.; Kirkland, J. J. *Introduction to Modern Liquid Chromatography*; Wiley-Interscience: New York, 1979.
(3) Pasch, H.; Trathnigg, B. *HPLC of Polymers*; Springer: Berlin, 1997.
(4) Barth, H. G.; Boyers, B. E.; Jackson, C. *Anal. Chem.* **1998**, *70*, 251.
(5) Casassa, E. F. *J. Polym. Sci., Polym. Lett. Ed.* **1967**, *5*, 773.
(6) Casassa, E. F.; Tagami, Y. *Macromolecules* **1969**, *2*, 14.

(7) Haller, W. *Macromolecules* **1977**, *10*, 83.
(8) Gorbunov, A. A.; Skvortsov, A. M. *Adv. Colloid Polym. Sci.* **1995**, *62*, 31.
(9) Davidson, M. G.; Suter, U. V.; Deen, W. M. *Macromolecules* **1987**, *20*, 1141.
(10) Wang, Y.; Teraoka, I. *Macromolecules* **1997**, *30*, 8473.
(11) Cifra, P.; Bleha, T.; Wang, Y.; Teraoka, I. *J. Chem. Phys.* **2000**, *113*, 8313.
(12) Colin, H. In *High Performance Liquid Chromatography;* Brown, P. R., Hartwick, R. A., Eds.; John Wiley: New York, 1989; Vol. 98, pp 415−478.
(13) Luo M.; Teraoka, I. *Macromolecules* **1996**, *29*, 4226.
(14) Teraoka, I. In *Column Handbook for Size Exclusion Chromatography*; Academic Press: San Diego, 1999.
(15) Teraoka, I.; Langley, K. H.; Karasz, F. E. *Macromolecules* **1993**, *26*, 287.
(16) Teraoka, I.; Zhou, Z.; Langley, K. H.; Karasz, F. E. *Macromolecules* **1993**, *26*, 6081.
(17) Lee, D.; Gong, Y.; Teraoka, I. *Macromolecules* **2002**, *35*, 7093.
(18) Satterfield, C. N.; Colton, C. K.; De Turckheim, B.; Copeland, T. M. *AIChE J.* **1978**, *24*, 937.
(19) Colton, C. K.; Satterfield, C. N.; Lai, C. J. *AIChE J.* **1975**, *21*, 289.
(20) Brannon, J. H.; Anderson, J. L. *J. Polym. Sci., Polym. Phys. Ed.* **1982**, *20*, 857.
(21) Dube, A.; Teraoka, I. *Macromolecules* **1997**, *30*, 7753.
(22) Rudin, A. *J. Polym. Sci., Polym. Phys. Ed.* **1971**, *9*, 2587.
(23) Bleha, T.; Mlýnek, J.; Berek, D. *Polymer* **1980**, *21*, 798.
(24) Fixman, M.; Peterson, J. M. *J. Am. Chem. Soc.* **1964**, *86*, 3524.
(25) Gland, D. E. *AIChE J.* **1981**, *27*, 51.
(26) Anderson, J. L.; Brannon, J. H. *J. Polym. Sci., Polym. Phys. Ed.* **1981**, *19*, 405.
(27) Thompson, A.; Gland, D. E. *Macromolecules* **1996**, *29*, 4314.
(28) Cifra, P.; Bleha, T.; Romanov, A. *Polymer* **1988**, *29*, 1664.
(29) Bleha, T.; Cifra, P.; Karasz, F. E. *Polymer* **1990**, *31*, 1321.
(30) Cifra, P.; Bleha, T. *Polymer* **2000**, *41*, 1003.
(31) Cifra, P.; Bleha, T. *Macromol. Theory Simul.* **2000**, *9*, 555.
(32) Cifra, P.; Bleha, T. *Macromolecules* **2001**, *34*, 605.
(33) Cifra, P.; Bleha, T. *Polymer* **2003**, *44*, 3745.
(34) Cifra, P.; Teraoka, I. *Macromolecules* **2003**, *36*, 9638.
(35) Skrinarova, Z.; Bleha, T.; Cifra, P. *Macromolecules* **2002**, *35*, 8896.
(36) Skrinarova, Z.; Cifra, P. *Macromol. Theory Simul.* **2001**, *10*, 523.
(37) Skrinarova, Z.; Cifra, P. *Macromol. Theory Simul.* **2002**, *11*, 401.
(38) Teraoka, I.; Wang, Y. *J. Chem. Phys.* **2001**, *115*, 1105.
(39) Teraoka, I.; Cifra, P. *J. Chem. Phys.* **2001,** *115*, 11362.
(40) Buta, D.; Freed, K. F.; Szleifer, I. *J. Chem. Phys.* **2000**, *112*, 6040.
(41) Fleer, G. J.; Cohen Stuart, M. A.; Scheutjens, J. M. H. M.; Cosgrove, T.; Vincent, B. *Polymers at Interfaces*; Chapman & Hall: London, 1993.
(42) Fleer, G. J.; Skvortsov, A. M.; Tuinier, R. *Macromolecules* **2003**, *36*, 7857.
(43) Eisenriegler, E. *J. Chem. Phys.* **1983**, *79*, 1052.
(44) Eisenriegler, E. *Polymers near Surfaces;* World Scientific: Singapore, 1993.
(45) De Gennes, P. G. *Scaling Concepts in Polymer Physics;* Cornell University Press: Ithaca, NY, 1979.
(46) Tuinier, R.; Vliegenhart, G. A.; Lekkerkerker, H. N. W. *J. Chem. Phys.* **2000**, *113*, 10768.
(47) Tuinier, R.; Fleer, G. J. *Macromolecules* **2004**, *37*, 8754, 8764.
(48) Tuinier, R.; Lekkerkerker, H. N. W. *Eur. Phys. J. E* **2001**, *6*, 129.
(49) Alexander-Katz, A.; Moreira, A. G.; Fredrickson, G. H. *J. Chem. Phys.* **2003**, *118*, 9030.
(50) In ref 11 only results for $D = 45$, 29, 19, 11, and 7 were presented. We thank P. Cifra for making available these numerical data and, in addition, those for $D = 5$.
(51) Asakura, S.; Oosawa, F. *J. Chem. Phys.* **1954**, *22*, 1255.
(52) Flory, P. J. *Principles of Polymer Chemistry*; Cornell University Press: Ithaca, NY, 1953.

MA047542B